EMBEDDED ATOM METHOD SIMULATIONS OF SINGLE CRYSTAL NICKEL DUCTILE FRACTURE

G.P. Potirniche[1], M. F. Horstemeyer[1, 2], G. J. Wagner[3], P. M. Gullett[3]

[1]Center for Advanced Vehicular Systems, Mississippi State University, MS
[2]Mechanical Engineering Department, Mississippi State University, MS
[3]Sandia National Laboratories, Livermore, CA

ABSTRACT

Molecular dynamics simulations of single crystal nickel were performed to analyze the influence of specimen size on ductile fracture. Uniaxial tension of four specimen sizes ranging from approximately 5,000 atoms to 170,000 atoms with the same initial void volume fraction was performed at high rates of deformation (10^8 – 10^{10}/sec). The 3D specimens were given a rectangular initial shape with uniform thickness and were provided with one and two cylindrical voids. Parameters quantifying damage evolution such as, post-initial yielding stress-strain behavior and void volume fraction evolution were computed as the voids grew and coalesced due to the increasing applied tractions. The results showed that the different specimen size changes the dislocation pattern, the void aspect ratio, and the stress-strain response of the specimens. From zero to 20% strain the void growth is dominated by dislocation nucleation that correlates with the size scale influence observed by Horstemeyer et al. [1]. Beyond 20% the size scale differences cease to be relevant because the effects of dislocation nucleation are overcome by dislocation interaction. This study provides the fodder for development of continuum damage mechanics phenomenological models for use in nanocrystalline materials.

1 INTRODUCTION

Nucleation, growth and coalescence of voids are the three mechanisms by which damage progression occurs leading to ductile failure in a wide range of engineering materials. Intrinsically, damage evolution is a multiscale process involving the above-mentioned mechanisms that have been extensively studied at the micro- and macroscales. However, at the nanoscale the void growth and void coalescence processes have not been satisfactorily studied and understood. In this study we focus on single voids growing and multiple voids coalescing at the nanoscale by using the embedded atom method (EAM) potentials in molecular dynamics simulations.

Previous research by Horstemeyer et al. [2] and Gall et al. [3] indicated that molecular dynamics can be used to study plastic deformation mechanisms and the phenomenon of ductile failure at the atomistic scale. Horstemeyer et al. [4] integrated EAM in a multiscale modeling approach and analyzed the intrinsic mechanical response of single crystals at three relevant material scales. The results indicated that the material length scale greatly influenced the stress-strain response arising from the importance of dislocation nucleation. By analyzing void growth mechanisms in copper single crystals using both EAM and crystal plasticity theory Farrissey et al. [5] found that while a qualitative similitude between void developments at atomic and crystallographic length scales exists, the atomistic simulations indicated that the stress levels predicted with EAM are larger than those predicted with crystal plasticity, consistent with the dislocation nucleation arguments of Horstemeyer et al. [1,2]. Makino et al. [6] simulated void formation in nickel single crystals using molecular dynamics by subjecting infinitely long cylinders to a multiaxial tensile strain field. Their work was chiefly concerned with void nucleation and stable void growth, and they found that above a critical value of the applied load, a void nucleated from vacancies in the crystalline lattice.

This work presents an investigation of the void growth and void coalescence mechanisms in different sized nickel single crystal specimens. The void volume fraction evolution was determined as a function of the applied strain for single and multiple void specimens.

2 EMBEDDED ATOM METHOD BACKGROUND

The EAM potentials employed in a computational framework can be used to determine the relationships between microstructure and mechanical properties at material scales ranging from the atomic to the continuum (Baskes and Johnson [6] and Baskes, 1994,1998 [7,8]).

The EAM potentials are based on molecular dynamics principles developed initially by Daw and Baskes [9]. EAM allows the calculation of the thermodynamic forces and stress tensors for the atoms in the lattice based on the notion of an embedded energy. The total energy of an atomic system, E, is calculated by summing the individual embedding energy F^i of each atom i in the atomic aggregate, as follows

$$E = \sum_i F^i\left(\sum_{j\neq i}\rho^i\left(r^{ij}\right)\right) + \frac{1}{2}\sum_{ij}\phi^{ij}\left(r^{ij}\right) \tag{1}$$

where, j is any neighboring atom, r^{ij} and ϕ^{ij} are the distance and the pair potential, respectively, between the atoms i and j.

At each atom i, the stress tensor is defined as a volume average of the dipole force tensor

$$\sigma_{mk} = \frac{1}{N^*}\sum_i^{N^*}\beta_{mk}^i \tag{2}$$

where N^* is the number of active atoms that participate in creating the stress in the lattice and β is the dipole force between neighboring atoms, which can be derived from the embedding energy.

3 RESULTS AND DISCUSSION

3.1 Void growth and coalescence

The governing equations of EAM were implemented in a multiprocessor code developed by Plimpton [10]. For the simulations, the specimens were created at four different sizes. The specimens represented a plate with one or two central holes subjected to uniaxial strain, and they are illustrated in Figure 1.

Geometrical dimensions corresponding to these four specimen sizes are indicated in Table 1. All the specimens were assigned the same thickness of 0.992 nm (4 unit cells). The specimen sizes were increased from 4,408 atoms (smallest length scale) to 171,376 atoms (largest length scale). The specimen edges were aligned with the global system of coordinates (xyz). The FCC crystalline lattice was aligned for all of the one-void and two-void specimens; that is, the x-axis corresponded to (1 0 0) direction, the y-axis corresponded to (0 1 1) direction and the z-axis corresponded to (0 – 1 1) direction. The applied tractions were exerted in the x-direction, up to a total true strain of $\varepsilon = 41\%$. All the simulations were run at a constant temperature of 300 K.

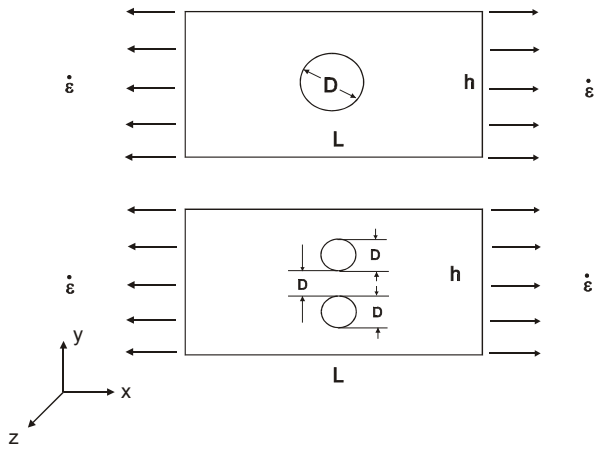

Figure 1: Geometry of void growth and coalescence specimens subjected to uniaxial tension at a constant strain rate

Figure 2(a) shows the uniaxial stress-strain response for the one-void specimen at 18,448 atoms comprises an elastic portion up to a true strain of 14.5% with a yield stress of 17.1 GPa. As the yield stress is reached, dislocations nucleate near the void due to the stress concentration.

Specimen	L (nm)	h (nm)	t (nm)	D(nm)	No. of atoms
1	8.448	6.4963	0.992	1.493	4,408
2	16.896	12.992	0.992	2.986	18,448
3	33.792	25.985	0.992	5.973	75,648
4	50.688	38.977	0.992	8.960	171,376

(a) Geometrical dimensions for one-void specimens

Specimen	L (nm)	h (nm)	t (nm)	D (nm)	No. of atoms
5	8.448	6.4963	0.992	1.056	5,052
6	16.896	12.992	0.992	2.112	19,748
7	33.792	25.985	0.992	4.224	78,140
8	50.688	38.977	0.992	6.336	175,172

(b) Geometrical dimensions for one-void specimens

Table 1: Geometrical dimensions of void coalescence specimen subjected to uniaxial tension under constant strain rate

As the void increases in size, the void volume fraction correspondingly increases. The aspect ratio of the hole changes noticeably due to dislocations being nucleated from the void and from the plastic spin that rotates the lattice at larger strains. Also, the stress resistance of the specimen decreases significantly to about 5 GPa at the final true strain of 41%. Severe necking of the specimen occurs starting at about 30% strain level. The aspect ratio of the void is highly

influenced by the dislocation pattern emanating from the hole and significantly different than the smaller specimens.

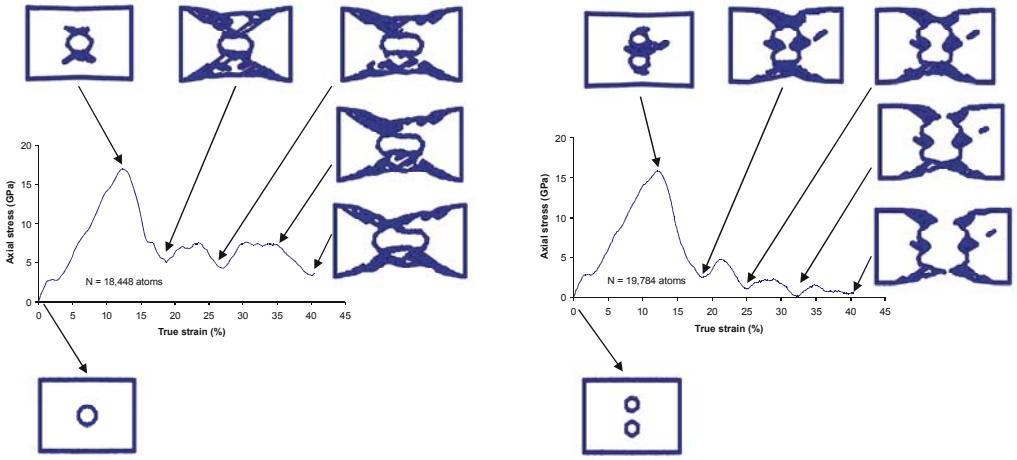

(a) (b)

Figure 2: Stress-strain response under uniaxial tension at a strain rate of 10^{10} /sec for (a) one-void and (b) two-void specimens

The increase in void volume fraction and dislocations nucleation induces an abrupt decrease in the capacity of the specimen to respond to stress due to uniaxial straining.

The results for the void coalescence effects for the 19749 atoms is presented in Figure 2(b). As the uniaxial stress reaches the yield stress, dislocations nucleated in the ligament region between the two voids. As the applied strain increased, the region between the two voids shrank, and the two voids collapsed to form one larger void. Concomitantly, dislocations nucleated toward the edges of the specimen, causing the initial necking of the tensile specimen. The stress-strain diagram also indicated that the largest drop in the stress-strain curve occurred as the voids coalesced to form one larger void. Furthermore, as the applied strain increased, the coalesced voids increased their volume. At the same time, nucleated slip patterns further decreased the stress resistance of the uniaxial specimen.

3.2 Void volume fraction evolution

The simulation results, shown in Figures 4(a) and 4(b) indicate that, for both the one-void specimens and two-void specimens, under increasing uniaxial strain, the void volume fraction (*f*) for the one-void specimens increased from 0.03 to a maximum value of approximately 0.15 up to approximately 20% strain. In general the smaller length scale specimen experienced an increased void-volume fraction resulting from larger elastic stresses. This void volume size scale effect could also be influenced by the differences in the dislocation nucleation processes. As the strain is increased to large plastic deformations, the specimen size effect diminished to the point where the four increasing length scale specimens present almost the same void volume fraction with respect to the applied uniaxial strain up to the final applied strain.

The void volume evolution for the two-void specimens is shown in Figure 4b, where the void volume fraction (*f*) evolution with respect to the applied uniaxial strain is presented for the two-void specimens. Comparing Figure 4(b) to Figure 4(a), the same conclusions can be inferred in the

case of two-void specimens as in the case of one-void specimens, suggesting that at this material level and at the strain rate considered the preponderant failure mechanism is void growth by dislocation nucleation and less by coalescence of voids.

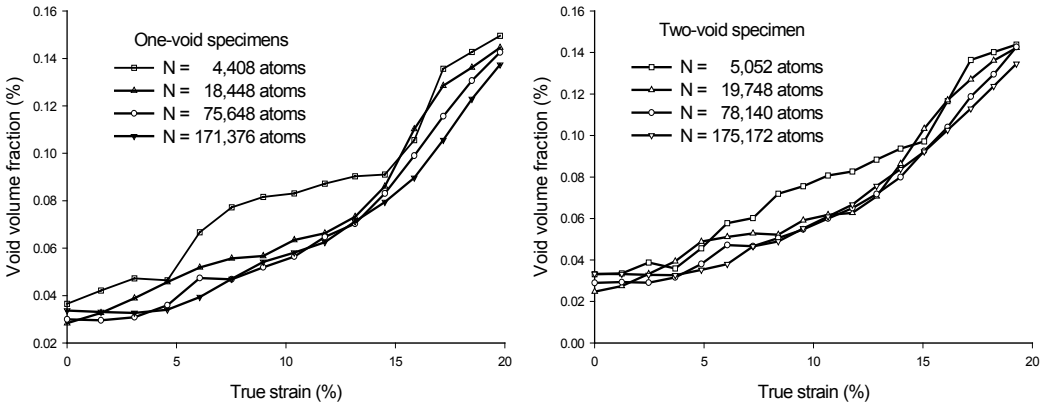

(a) (b)

Figure 4: Void volume fraction evolution at increasing length scales for (a) one-void specimens and (b) two-void specimens

3.3 Strain rate effects

Stress-strain behavior for the one-void and two-void specimens was compared for three strain rates levels: 10^8/sec, 10^9/sec and 10^{10}/sec. For the one-void specimens, Figure 11a shows that, as the strain rate increased two orders of magnitude, the yield stress increased from 15 GPa to 20.5 GPa. Correspondingly, the elastic strain at which first yielding of the specimen occurred, increased with increasing strain rate.

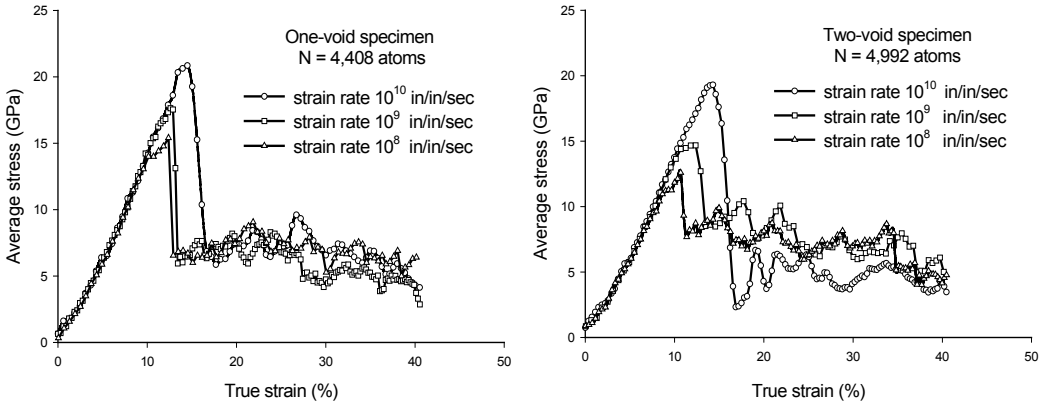

(a) (b)

Figure 5: Stress-strain response at various strain rates for (a) one-void and (b) two-void specimens

After the initial yielding, the stress-strain response decreased significantly. Toward final fracture, the lowest stress-strain resistance is exhibited by the specimen that was subjected to the lowest strain rate.

4 CONCLUSIONS

Molecular dynamics simulations showing damage evolution at four increasing specimen sizes were performed to study the evolution of void growth and coalescence under very high strain rates. One-void and two-void specimens were increased in size to represent an increasing length scale. The study revealed that the void growth occurs due to the crystallographic plastic slip initiated at the hole as a consequence of the stress concentration and propagated toward the outer edges of the specimen. The differences in plastic slip nucleation pattern indicated a varying void shape evolution at increasing material length scale. For the two void specimens, the study revealed that the configuration of plastic slip also influenced the void coalescence mechanism, depending on the specimen size (length scale). The averaged axial stress-strain response clearly indicated a length scale effect regardless of the number of voids. The smallest specimen size (length scale) exhibited the largest yield stress. The void volume fraction for the one-void specimen and two-void specimens was shown to increase as the remotely applied traction increased similarly to macroscopic observations.

5 ACKNOWLEDGEMENTS

The authors are grateful to the Center for Advanced Vehicular Systems at Mississippi State University for supporting this study.

6 REFERENCES

1. Horstemeyer, M. F., Baskes, M. I., Plimpton S. J. Length scale and time scale effects on the plastic flow of FCC metals. Acta Mater. 49, pp. 4363-4374, 2001

2. Horstemeyer M. F., Baskes M. I., Plimpton S. J. Computational nanoscale plasticity simulations using embedded atom potentials. Teoretical and Applied Fracture Mechanics 37, pp. 49-98, 2001

3. Gall, K., Horstemeyer M. F., Van Schilfgaarde M., Baskes M. I. Atomistic simulations on the tensile debonding of an aluminum-silicon interface. J. Mech. Phys. Solids. 48, pp. 2183-2212, 2000

4. Farrissey L, Ludwig M, McHugh PE, Schmauder S. An atomistic study of void growth in single crystalline copper. Computational Material Science. 18, pp. 102-117, 2000

5. Makino M., Tsuji T., Noda N. MD simulation of atom-order void formation in Ni FCC metal. Computational Mechanics. 26(3), pp. 281-287, 2000

6. Baskes M. I. Johnson R. A. Modified Embedded Atom Potentials for HCP Metals. Modelling Simul. Mater. Sci. Eng. 2, pp. 147-163, 1994

7. Baskes M. I. The Modified Embedded Atom Method. Computational Material Modeling, AD-Vol. 42/PVP-Vol. 294, pp. 23-35, 1994

8. Baskes M. I. Determination of modified Embedded Atom Method parameters for Nickel. Materials Chemistry and Physics 50, pp. 152-158, 1997

9. Daw M.S., and Baskes M. I. Embedded-atom method: derivation and application to impurities, surfaces, and other defects in metals. Phys. Rev. B 29, p. 6443,1984

10. Plimpton S. Fast parallel algorithms for short-range molecular dynamics. J Comp Phys, 117, pp. 1-19, 1995